Characterization of the ^{163}Ho Electron Capture Spectrum: A Step Towards the Electron Neutrino Mass Determination

P. C.-O. Ranitzsch,* C. Hassel, M. Wegner, D. Hengstler, S. Kempf, A. Fleischmann, C. Enss, and L. Gastaldo
Kirchhoff-Institute for Physics, Heidelberg University, 69120 Heidelberg, Germany

A. Herlert† and K. Johnston‡
Physics Department, CERN, 1211 Geneva 23, Switzerland

(Received 26 April 2017; revised manuscript received 17 July 2017; published 19 September 2017)

The isotope ^{163}Ho is in many ways the best candidate to perform experiments to investigate the value of the electron neutrino mass. It undergoes an electron capture process to ^{163}Dy with an energy available to the decay, Q_{EC}, of about 2.8 keV. According to the present knowledge, this is the lowest Q_{EC} value for such transitions. Here we discuss a newly obtained spectrum of ^{163}Ho, taken by cryogenic metallic magnetic calorimeters with ^{163}Ho implanted in the absorbers and operated in anticoincident mode for background reduction. For the first time, the atomic deexcitation of the ^{163}Dy daughter atom following the capture of electrons from the 5s shell in ^{163}Ho, the OI line, was observed with a calorimetric measurement. The peak energy is determined to be 48 eV. In addition, a precise determination of the energy available for the decay $Q_{EC} = (2.858 \pm 0.010_{stat} \pm 0.05_{syst})$ keV was obtained by analyzing the intensities of the lines in the spectrum. This value is in good agreement with the measurement of the mass difference between ^{163}Ho and ^{163}Dy obtained by Penning-trap mass spectrometry, demonstrating the reliability of the calorimetric technique.

DOI: 10.1103/PhysRevLett.119.122501

Experiments investigating neutrino oscillations over short and long baselines are achieving very high precision on parameters composing the Pontecorvo-Maki-Nakagawa-Sakata matrix and on the difference between the squared mass states [1–3]. Besides the fact that neutrino oscillations imply neutrinos are massive particles, the mentioned experiments are not suitable to determine the absolute neutrino mass scale. Therefore, a wide range of different approaches are pursued to pin down the neutrino mass. The study of the distribution of mass in the Universe is sensitive to the sum of neutrino masses $m_{tot} = \sum m_i$ and provides stringent limits $m_{tot} < 1$ eV [4,5]. The rate of the neutrinoless double beta decay is a function of the effective Majorana mass $m_{\beta\beta} = |\sum U_{ei}^2 m_i|$. By setting a lower limit on the half-life for such a process, corresponding upper limits on $m_{\beta\beta}$ ranging from 0.1–0.4 eV have been reported [6–8]. The analysis of the kinematics of low-energy beta decays and electron capture (EC) processes are used to determine the effective mass of the electron (anti)neutrino $m_{eff}^2(\nu_e) = \sum |U_{ei}^2| m_i^2$ in a model-independent way, since just energy and momentum conservation are utilized. In both processes, the shape of the measured spectrum is proportional to the phase-space factor, which is a function of the neutrino mass. Therefore, in both cases, the endpoint region of the spectrum is mostly affected by the neutrino mass. At present, two nuclides are favored for such direct neutrino mass experiments: ^{3}H undergoing β-decay [9–11] and ^{163}Ho decaying through EC [12–14] with the aim of achieving sub-eV sensitivity on the electron (anti)neutrino mass. In both cases the neutrino mass affects the shape of the spectrum in the endpoint region. So far, the best limits have been achieved for the electron antineutrino mass based on ^{3}H, $m_{eff}(\nu_e) < 2.3$ eV [15] and $m_{eff}(\nu_e) < 2.12$ eV [16].

The isotope ^{163}Ho has an energy available to the decay, Q_{EC}, of about 2.8 keV. This is the lowest known Q_{EC} value and makes ^{163}Ho the best candidate for the investigation of the electron neutrino mass by the analysis of an EC spectrum. Recently the energy available to the EC process in ^{163}Ho was precisely determined, by Penning-trap mass spectrometry, to be $Q_{EC} = (2.833 \pm 0.030_{stat} \pm 0.015_{syst})$ keV [17]. This measurement is important not only because of the small uncertainties, but mainly because it was obtained as the difference between the mass of the parent ^{163}Ho atom and the mass of the daughter ^{163}Dy atom; this method does not depend on the decay modes of ^{163}Ho, contrary to all previous Q_{EC} measurements [18–21].

De Rújula and Lusignoli proposed in 1982 that, in the case of ^{163}Ho, it is possible to reach high sensitivity to a nonzero electron neutrino mass if all the energy released in the decay, besides the energy taken away by the electron neutrino, is measured [22]. This method allows for a reduction of systematic uncertainties with respect to experiments where only the x-ray spectrum is measured

[20,23–26], since it does not require the knowledge of x-ray emission branching ratios and corrections due to radiation absorption in the source itself or in nonactive parts of the detector. In fact, the capture of $3s$ electrons leads to one resonance, the MI line, in the calorimetrically measured spectrum (see Fig. 4 in [27]), while in an x-ray spectrum the same captures lead to a sum of resonances due to several radiative transitions in decay cascades (see Fig. 7 in [24]).

Recently we have shown that the EC spectrum of ^{163}Ho can be measured with high precision using low temperature metallic magnetic calorimeters (MMCs) [28,29]. These results motivated the formation of the international collaboration ECHo (Electron Capture in ^{163}Ho Experiment) with the aim of investigating the electron neutrino mass in the sub-eV range by means of the high-precision and high-statistics calorimetric measurement of the EC spectrum of ^{163}Ho [12]. Meanwhile, two other international collaborations have been established, HOLMES (Electron Capture Decay of ^{163}Ho to Measure the Electron Neutrino Mass with sub-eV sensitivity) [13] and NuMECS (Neutrino Mass via ^{163}Ho Electron Capture Spectroscopy) [14], that follow a similar approach based on cryogenic detectors. For all these projects, it is necessary to determine the parameters of the ^{163}Ho EC spectrum with high precision. Here we will discuss a newly obtained spectrum taken with MMC detectors that allows for the determination of several of these parameters with unprecedented precision in a cryogenic experiment.

The MMCs used in this experiment are energy-dispersive detectors operated at temperatures below 100 mK [30,31]. They are characterized by a paramagnetic temperature sensor, typically Au or Ag doped with Er at a concentration of a few hundred ppm, positioned in a weak magnetic field of the order of ∼mT. The sensor is tightly connected to a particle absorber and weakly connected to the thermal bath. The deposition of energy into the absorber generates a temperature rise in the detector, leading to a change of magnetization of the sensor, which is read out by a low-noise high-bandwidth dc Superconducting Quantum Interference Device (SQUID). The resolving power $E/\Delta E$ of these detectors approaching 5000, the intrinsic response time well below 1 μs, and the excellent linearity make MMCs attractive for the high-precision measurement of the ^{163}Ho spectrum [32].

The first MMC chip prototype we have developed for these measurements consists of four individual detector pixels, positioned on one silicon chip of 5×5 mm^2. The detailed design and the performance of the detector have been described in [29]. The layout is based on the double-meander geometry [31]. Only one wing of each gradiometric double meander was equipped with a sensor and an absorber. The ^{163}Ho source was enclosed into the Au absorber via online ion implantation, which was performed at ISOLDE-CERN [33], and yielded a total activity per pixel of $A \approx 0.01$ Bq. The absorbers were designed in such a way that the source is surrounded in each direction by at least 5 μm of gold, ensuring a quantum efficiency close to 100% for the energy emitted in the EC decay of ^{163}Ho. The detector was mounted at the mixing chamber of a dilution refrigerator with base temperature of $T = 20$ mK and was operated at a chip temperature of $T = 29$ mK.

The ^{163}Ho spectrum was obtained by simultaneously measuring two of the four pixels. Each of them was read out with an integrated two-stage SQUID of the type C6X114W produced by the Physikalisch-Technische Bundesanstalt PTB in Berlin [34]. The output signal of the SQUIDs, after being amplified by a room-temperature electronics [35], was split into two channels. One of them, used as a trigger, was strongly band-pass filtered, while the other was only low-pass filtered to prevent aliasing and was recorded as a trace for offline analysis. All resulting four channels were digitized by a four-channel 14-bit digitizer [36]. Whenever one of the two trigger signals exceeded the trigger level, both traces were acquired on the same time window. The synchronization of the data acquisition for the two pixels allowed for a coincidence analysis.

Since only one of the wings of the double meander of each detector was covered with a Au:Er film, the detectors were highly sensitive to temperature changes in the silicon substrate. Because of that, an event in one pixel leads to a signal via thermal cross talk in the neighboring pixels having an amplitude corresponding to about 1% of the signal in the primary detector. Note, however, that for events due to the EC in ^{163}Ho, the cross-talk signals are below the detection threshold of 30 eV. Thus, the sensitivity to the substrate temperature allowed us to distinguish three types of signals: (1) events caused by a direct energy deposition in one pixel, where only one detector registers a signal, (2) events where a sufficiently large energy is deposited in one pixel so that a thermal cross-talk signal in the neighboring pixels is observed, and (3) events due to particles interacting in the substrate and causing a slow rising signal in all detectors.

Obviously, these three kinds of signals have different pulse shapes. Using just pulse-shape discrimination, it is possible to distinguish the three families down to an energy of about 300 eV. For smaller energies the signal-to-noise ratio is not sufficient to safely separate all three classes. However, substrate and cross-talk events give rise to a coincident signal in all four detectors. By synchronizing data acquisition of the two pixels, anticoincidence can be used to select direct events in a detector. Figure 1 shows a scatter plot where the amplitude of channel 1 is plotted versus the amplitude of channel 0. The events showing vanishing amplitudes in either channel 0 or channel 1 correspond to direct events in the opposite channel, while the events scattering around the diagonal belong to the two background classes just discussed.

By selecting only the direct events in channel 0 and channel 1 and summing several of such measurements, the spectrum showed in Fig. 2 has been obtained. The background events can be clearly eliminated down to about 150 eV. Below this threshold, a small number of background events survives the cut and an exponential function is used to describe this background, as shown in Fig. 2 as the grey shaded region.

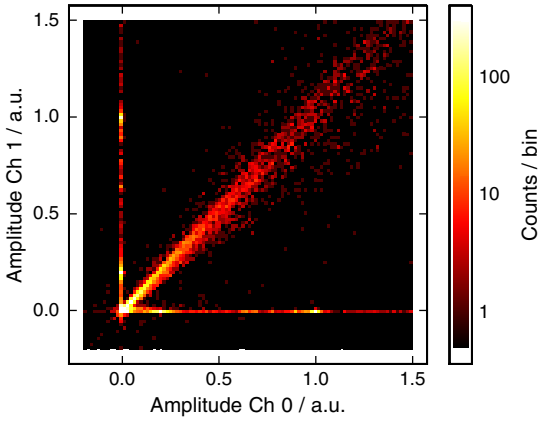

FIG. 1. The amplitude of the events in channel 1 plotted versus the amplitude of the events in channel 0. The number of counts per bin for all possible combinations in the defined plane is given by the color code shown on the right.

In order to analyze this spectrum we use a simplified model in which just first-order excited states in ^{163}Dy, characterized by one hole left by the captured electron and one $4f$ electron, are considered. In this case the differential spectrum can be written as

$$\frac{dW}{dE_c} = \mathcal{C}(Q_{\mathrm{EC}} - E_c)^2 \sqrt{1 - \frac{m_\nu^2}{(Q_{\mathrm{EC}} - E_c)^2}} \times \sum_H \frac{B_H \varphi_H^2(0) \Gamma_H}{2\pi[(E_c - E_H)^2 + \Gamma_H^2/4]}. \quad (1)$$

Here, m_ν is the effective electron neutrino mass. The natural Lorentzian line shape of the different spectral lines H is characterized by the line central energy E_H, the intrinsic linewidth Γ_H, and the amplitude, which is given by the squared electron wave function at the nucleus $\varphi_H^2(0)$ multiplied by the overlap and exchange correction B_H of the order of a few percent [37]. The value $\mathcal{C}$ is a constant.

The peak energies E_H and the intrinsic linewidths Γ_H of four resonances in the ^{163}Ho spectrum corresponding to the MI($3s$), MII($3p_{1/2}$), NI($4s$), and NII($4p_{1/2}$) lines, have been determined in a previous experiment to a precision of $\Delta E_H < 1.0$ eV and $\Gamma_H < 1.0$ eV, given by uncertainties on the calibration and the fit [38]. This experiment used the same detectors as for the reported measurement and an external ^{55}Fe source for calibration. The parameters are summarized in Table I, together with the binding energies E_H^{bin} of the captured electrons with respect to the Dy atom, and literature values of the linewidths Γ_H^{lit} for comparison [39]. Note that there is a systematic shift of the experimental peak positions to lower energies when compared to the electron binding energies of the daughter atom. Such a difference is expected due to the presence of the additional $4f$ electron in the dysprosium shell after the electron capture. The peak energies can be given in first approximation by $E_H \approx E_H^{\mathrm{bin}} - E_{4f}$ [24]. At the same time, the linewidths Γ_H derived from fitting the spectrum agree well with the expected and previously reported values. Only the width of the NII line is significantly broader in our measurement. At this point we do not know the origin of this surprising discrepancy.

The parameters E_H^{exp} and Γ_H^{lit} have been used as input to analyze the new reported spectrum; therefore, no additional calibration source was necessary. The spectrum shown in Fig. 2 was obtained by summing 28 single spectra, acquired in the synchronized mode. The line shapes are given by the convolution of the intrinsic line shapes, as defined by Eq. (1) and the detector response, well described by a Gaussian modified by an exponential function towards low energies, which accounts for energy losses caused by athermal phonons. These are created in the first phase of the energy deposition in the absorber and can reach the solid substrate without depositing their energy in the detector [43]. Note that this effect can be reduced by minimizing the contact area between the absorber and temperature sensor, as demonstrated for MMCs in [27,31]. The detector used here did not have such a reduced contact area and, therefore, around 10% of the events are affected by this energy loss mechanism.

The analysis of the summed spectrum resulted in an instrumental linewidth $E_{\mathrm{FWHM}} = 8.3$ eV. Under optimal conditions the detectors at 29 mK have an expected energy resolution of $\Delta E_{\mathrm{FWHM}} = 6$ eV. The reason for the slightly worse energy resolution can be explained by a somewhat higher readout noise than expected.

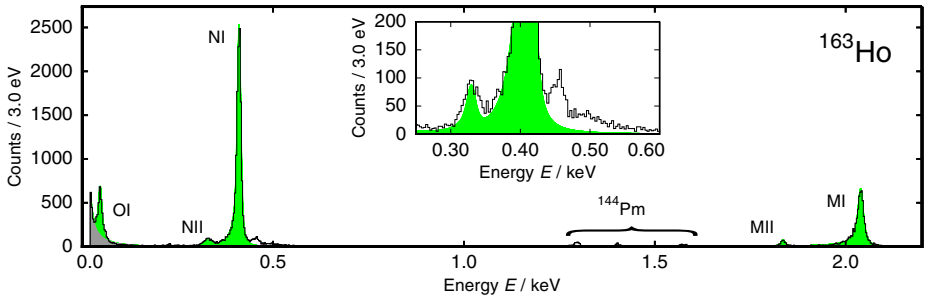

FIG. 2. Measured ^{163}Ho EC spectrum (black histogram) and the theoretical description (green filled area). The background contribution that survived the cuts is shown in grey. In addition to the five lines of the ^{163}Ho spectrum, three lines due to ^{144}Pm EC can be seen. The latter was coimplanted with the desired ^{163}Ho. The insert shows a magnification of the N-lines region which emphasizes the presence of additional structure in the spectrum due to higher-order excited states in ^{163}Dy.

TABLE I. The parameters used in or resulting from the fit to the measured spectrum in Fig. 2. A detailed description of the parameters can be found in the text. Additionally, the number of events n_H^{exp} in the measurement per line is given.

H	MI	MII	NI	NII	OI
$(B_H/B_{\mathrm{MI}})\times(\varphi_H^2(0)/\varphi_{\mathrm{MI}}^2(0))$ [37]	1	0.051	0.244	0.012	0.032
E_H^{bin}/eV [40]	2046.9	1844.6	420.3	340.6	49.9 [41]
E_H^{exp}/eV	2040	1836	411.1	330.3	48
Γ_H^{lit}/eV [39]	13.2	6.0	5.4	5.3	3.7 [42]
Γ_H^{exp}/eV	13.4	4.8	4.7	13	5.6
n_H^{exp}	6334	449	13814	987	2442

Let us now turn to the discussion of the observed spectrum. Besides the lines from the ^{163}Ho electron capture, three lines due to ^{144}Pm electron capture can also be seen around 1.5 keV. This impurity was ion implanted as ^{144}PmF$^+$ of mass 163 u alongside the desired ^{163}Ho [29]. Four of the lines associated with the EC of ^{163}Ho (MI, MII, NI, and NII) have been observed in previous experiments [28,38]. The novel anticoincidence discrimination used in this analysis has made possible for the first time the observation and characterization of the deexcitation peak due to electron capture from ^{163}Ho $5s$ shells, the OI line, at an energy of $E = 48$ eV and with an intrinsic linewidth of $\Gamma_{\mathrm{OI}} = 5.6$ eV. As expected, the peak energy is shifted, with respect to the binding energy of $5s$ electrons in ^{163}Dy, to lower values. However, we would like to point out that this shift is significantly smaller than for all other lines and may point to interesting additional atomic physics effects not incorporated in the present description.

The simplified theoretical model, including only first-order transitions described by the parameters given in Table I, successfully describes the spectrum shown in Fig. 2, as indicated by the green areas. It only fails to describe the events around $E = 450$ eV, as can be well seen in the inset in Fig. 2. Since background can be ruled out as an explanation, we have to assume that the origin is related to EC processes in ^{163}Ho. In fact, recent theoretical models point to additional features in the spectrum due to higher-order excited states in ^{163}Dy generated during EC in ^{163}Ho, which can be described as states with two or three holes in the dysprosium shells [44–47]. However, at this point a quantitative agreement of data and theory is still lacking, indicating that the theoretical description of the higher-order processes is incomplete.

Because of the relatively low statistics and the fact that we cannot discriminate deexcitation with x rays from deexcitation where only electrons are involved, we cannot deduce any information on the Interal Bremsstrahlung in Electron Capture (IBEC) spectrum, as discussed in [24], by analyzing our data.

Finally, in order to obtain the Q_{EC} value from the analysis of the new ^{163}Ho spectrum, we consider that the amplitude of each line depends on the phase-space value at the peak energy. Therefore, the number of counts in each resonance, n_H, can be written as a function of Q_{EC}, under the assumption that neutrinos are massless and that only first-order excited states in ^{163}Dy are considered,

$$n_H = \mathcal{C}(Q_{\mathrm{EC}} - E_H)^2 \varphi_H^2(0) B_H. \quad (2)$$

The number of events n_H for each deexcitation line is calculated using the fit function, obtained by the convolution between the intrinsic line shape defined by Eq. (1), and integrating the single lines, as reported in Table I. To extract Q_{EC} it is convenient to fit the value given by the square root of the number of events in each line divided by $\varphi_H^2(0)$ and B_H, which is the value of the phase-space term at the peak energy of the line, as a function of E_H, according to

$$\sqrt{\frac{n_H}{\varphi_H^2(0) B_H}} = \sqrt{\mathcal{C}}(Q_{\mathrm{EC}} - E_H). \quad (3)$$

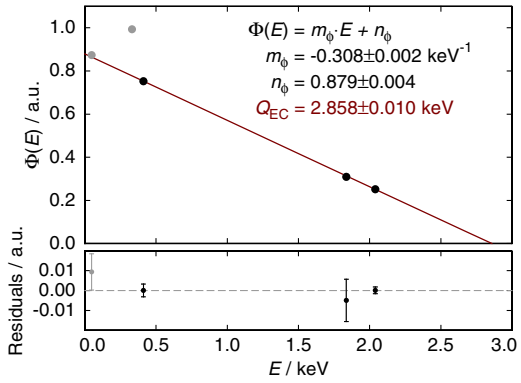

FIG. 3. The calculated phase-space factors for the Q_{EC} evaluation. Only the black data points enter into the linear fit. The lower plot shows the residuals from the fit and the statistical errors.

Only the MI, MII, and NI lines have been used to obtain the Q_{EC} value, since their large amplitudes make them the least affected by background or possible unknown systematics while still covering most of the energy range. The NII line is not included because it suffers from a large linewidth that is not understood, and the OI line is not included because of the additional background cut. Figure 3 shows the phase-space factor calculated using the number of events in each line n_H as a function of E_H with a linear fit. The point at which the fit crosses the energy axis gives the energy available for EC in ^{163}Ho of $Q_{\mathrm{EC}} = (2.858 \pm 0.010)$ keV. While only the MI, MII, and NI lines, weighted by their statistical uncertainties, are included in the fit, the OI line agrees with the fit rather well, while the NII line shows a significant deviation. This result supports the assumption that the shape description for the NII line is currently incomplete, which will be addressed in future measurements and theoretical investigations. The systematic uncertainty on Q_{EC} is governed by the uncertainty on the capture probabilities $\varphi_H^2(0)B_H$, which are based on theoretical calculations. Assuming a systematic error of 5% on the values given in Table I, which also includes

uncertainties related to the insufficient understanding of higher-order excited states in ^{163}Dy, the analysis leads to

$$Q_{\mathrm{EC}} = (2.858 \pm 0.010_{\mathrm{stat}} \pm 0.05_{\mathrm{syst}})\ \mathrm{keV}. \quad (4)$$

In summary, we presented a new high-precision measurement of the ^{163}Ho electron capture spectrum with an energy resolution of $\Delta E_{\mathrm{FWHM}} = 8.3$ eV obtained with metallic magnetic calorimeters making use of synchronized acquisition. The ^{163}Ho source has been enclosed in the detectors by ion implantation at ISOLDE-CERN. For the first time, the deexcitation from electron captures of $5s$ electrons was observed in a calorimetric experiment showing a peak at $E_{\mathrm{OI}} = 48$ eV with an intrinsic linewidth of $\Gamma_{\mathrm{OI}} = 5.6$ eV. This extends the description of the ^{163}Ho EC spectrum towards lower energies and, thus, allows not only for a more reliable energy calibration of future spectra, but also strengthens the quantitative understanding of the spectrum. The analysis of the relative amplitudes of the measured resonances allowed for the determination of the energy available to the electron capture in ^{163}Ho. The obtained value $Q_{\mathrm{EC}} = (2.858 \pm 0.010_{\mathrm{stat}} \pm 0.05_{\mathrm{syst}})$ keV agrees very well with the value obtained by Penning trap mass spectrometry and underscores again the validity of the calorimetric method using MMCs. In particular, it proves that the self-calibration of the ^{163}Ho spectrum, together with the excellent linearity of MMCs, allows for a precise definition of the energy scale at the endpoint region of the spectrum, which is of importance for the neutrino mass determination.

We would like to thank the Innovation Fund FRONTIER of Heidelberg University for providing the initial funding of this project. We acknowledge technical support by T. Wolf and the cleanroom team of the Kirchhoff Institute for Physics of Heidelberg University as well as by the ISOLDE team at European Organization for Nuclear Research (CERN) for fabrication of the detector chips and for the enclosing of the ^{163}Ho source. Part of this research was performed in the framework of the Deutsche Forschungsgemeinschaft (DFG) Research Unit FOR2202 Neutrino Mass Determination by Electron Capture in ^{163}Ho, ECHo (funding under Grants No. GA2219/2-1 and No. EN299/7-1).

*Present address: Institute fuer Kernphysik, Westfaelische-Wilhelms-Universitaet Muenster, 48149 Muenster, Germany. philipp.ranitzsch@uni-muenster.de

†Present address: FAIR GmbH, Planckstrasse 1, D-64291 Darmstadt, Germany.

‡Also at Technische Physik, Universitaet des Saarlandes, 66041 Saarbruecken, Germany.

[1] B. T. Cleveland, T. Daily, J. Raymond Davis, J. R. Distel, K. Lande, C. K. Lee, P. S. Wildenhain, and J. Ullman, Astrophys J. **496**, 505 (1998).

[2] Y. Fukuda *et al.* (Super-Kamiokande Collaboration), Phys. Rev. Lett. **81**, 1562 (1998).

[3] Q. R. Ahmad *et al.* (SNO Collaboration), Phys. Rev. Lett. **89**, 011301 (2002).

[4] C. L. Bennett *et al.* (WMAP Collaboration), Astrophys. J. Suppl. Ser. **208**, 20 (2013).

[5] P. A. R. Ade *et al.* (Planck Collaboration), Astron. Astrophys. **594**, A13 (2016).

[6] M. Agostini *et al.* (GERDA Collaboration), Phys. Rev. Lett. **111**, 122503 (2013).

[7] EXO-200 Collaboration, Nature (London) **510**, 229 (2014).

[8] A. Gando *et al.* (KamLAND-Zen Collaboration), Phys. Rev. Lett. **110**, 062502 (2013).

[9] J. Angrik *et al.* (KATRIN Collaboration), Forschungszentrum Karlsruhe GmbH Report No. FZKA 7090 (2005).

[10] D. M. Asner *et al.* (Project 8 Collaboration), Phys. Rev. Lett. **114**, 162501 (2015).

[11] S. Betts *et al.* (PTOLEMY Collaboration), arXiv:1307.4738.

[12] L. Gastaldo *et al.*, Eur. Phys. J. Spec. Top. **226**, 1623 (2017).

[13] B. Alpert *et al.*, Eur. Phys. J. C **75**, 112 (2015).

[14] M. P. Croce, M. W. Rabin, V. Mocko, G. J. Kunde, E. R. Birnbaum, E. M. Bond, J. W. Engle, A. S. Hoover, F. M. Nortier, A. D. Pollington, W. A. Taylor, N. R. Weisse-Bernstein, L. E. Wolfsberg, J. P. Hays-Wehle, D. R. Schmidt, D. S. Swetz, J. N. Ullom, T. E. Barnhart, and R. J. Nickles, J. Low Temp. Phys. **184**, 958 (2016).

[15] C. Kraus, B. Bornschein, L. Bornschein, J. Bonn, B. Flatt, A. Kovalik, B. Ostrick, E. Otten, J. Schall, T. Thümmler, and C. Weinheimer, Eur. Phys. J. C **40**, 447 (2005).

[16] V. N. Aseev, A. I. Belesev, A. I. Berlev, E. V. Geraskin, A. A. Golubev, N. A. Likhovid, V. M. Lobashev, A. A. Nozik, V. S. Pantuev, V. I. Parfenov, A. K. Skasyrskaya, F. V. Tkachov, and S. V. Zadorozhny, Phys. Rev. D **84**, 112003 (2011).

[17] S. Eliseev, K. Blaum, M. Block, S. Chenmarev, H. Dorrer, C. E. Düllmann, C. Enss, P. E. Filianin, L. Gastaldo, M. Goncharov, U. Köster, F. Lautenschläger, Y. N. Novikov, A. Rischka, R. X. Schüssler, L. Schweikhard, and A. Türler, Phys. Rev. Lett. **115**, 062501 (2015).

[18] E. Laegsgaard, J. U. Andersen, G. J. Beyer, A. De Rújula, P. G. Hansen, B. Jonson, and H. L. Ravn, in *Proceedings of the 7th International Conference on Atomic Masses and Fundamental Constants AMCO-7*, edited by O. Klepper, THD Schriftenreihe Wissenschaft und Technik Vol. 26 (Technische Hochschule Darmstadt, Darmstadt-Seeheim, 1984), pp. 652–658.

[19] F. Hartmann and R. Naumann, Nucl. Instrum. Methods Phys. Res., Sect. A **313**, 237 (1992).

[20] S. Yasumi, H. Maezawa, K. Shima, Y. Inagaki, T. Mukoyama, T. Mizogawa, K. Sera, S. Kishimoto, M. Fujioka, K. Ishii, T. Omori, G. Izawa, and O. Kawakami, Phys. Lett. B **334**, 229 (1994).

[21] F. Gatti, P. Meunier, C. Salvo, and S. Vitale, Phys. Lett. B **398**, 415 (1997).

[22] A. De Rújula and M. Lusignoli, Phys. Lett. **118B**, 429 (1982).

[23] C. Bennett, A. Hallin, R. Naumann, P. Springer, M. Witherell, R. Chrien, P. Baisden, and D. Sisson, Phys. Lett. **107B**, 19 (1981).

[24] P. T. Springer, C. L. Bennett, and P. A. Baisden, Phys. Rev. A **35**, 679 (1987).

[25] S. Yasumi, G. Rajasekaran, M. Ando, F. Ochiai, H. Ikeda, T. Ohta, P. Stefan, M. Maruyama, N. Hashimoto, M. Fujioka,

K. Ishii, T. Shinozuka, K. Sera, T. Omori, G. Izawa, M. Yagi, K. Masumoto, and K. Shima, Phys. Lett. **122B**, 461 (1983).
[26] S. Yasumi *et al.*, Phys. Lett. B **181**, 169 (1986).
[27] C. Hassel *et al.* (ECHo Collaboration), J. Low Temp. Phys. **184**, 910 (2016).
[28] P. C. -O. Ranitzsch, J.-P. Porst, S. Kempf, C. Pies, S. Schäfer, D. Hengstler, A. Fleischmann, C. Enss, and L. Gastaldo, J. Low Temp. Phys. **167**, 1004 (2012).
[29] L. Gastaldo, P.-O. Ranitzsch, F. von Seggern, J.-P. Porst, S. Schäfer, C. Pies, S. Kempf, T. Wolf, A. Fleischmann, C. Enss, A. Herlert, and K. Johnston, Nucl. Instrum. Methods Phys. Res., Sect. A **711**, 150 (2013).
[30] A. Fleischmann, C. Enss, and G. M. Seidel, in *Cryogenic Particle Detection*, edited by C. Enss, Topics in Applied Physics Vol. 99 (Springer-Verlag Berlin, Heidelberg, 2005), Chap. 4, pp. 151–216.
[31] A. Fleischmann, L. Gastaldo, S. Kempf, A. Kirsch, A. Pabinger, C. Pies, J.-P. Porst, P. Ranitzsch, S. Schäfer, F. v. Seggern, T. Wolf, C. Enss, and G. M. Seidel, AIP Conf. Proc. **1185**, 571 (2009).
[32] C. Pies, S. Schäfer, S. Heuser, S. Kempf, A. Pabinger, J.-P. Porst, P. Ranitsch, N. Foerster, D. Hengstler, A. Kampkötter, T. Wolf, L. Gastaldo, A. Fleischmann, and C. Enss, J. Low Temp. Phys. **167**, 269 (2012).
[33] E. Kugler, Hyperfine Interact. **129**, 23 (2000).
[34] SQUIDs by Physikalish-Technische Bundesanstalt, Institut Berlin, Abbestraße 2-12, D-10587 Berlin, Germany.
[35] SQUID electronics type XXF-1 from Magnicon GmbH, Barkhausenweg 11, D-22339 Hamburg, Germany.
[36] CompuScope Razor 14X2 CSE1442 A/D card by GaGe Applied Technologies, 900 N. State Street, Lockport, Illinois 60441, USA.
[37] A. Faessler, L. Gastaldo, and F. Šimkovic, J. Phys. G **42**, 015108 (2015).
[38] L. Gastaldo, K. Blaum, A. Doerr, C. Düllmann, K. Eberhardt, S. Eliseev, C. Enss, A. Faessler, A. Fleischmann, S. Kempf, M. Krivoruchenko, S. Lahiri, M. Maiti, Y. Novikov, P.-O. Ranitzsch, F. Simkovic, Z. Szusc, and M. Wegner, J. Low Temp. Phys. **176**, 876 (2014).
[39] J. Campbell and T. Papp, At. Data Nucl. Data Tables **77**, 1 (2001).
[40] R. D. Deslattes, E. G. Kessler, P. Indelicato, L. de Billy, E. Lindroth, and J. Anton, Rev. Mod. Phys. **75**, 35 (2003).
[41] A. Thompson *et al.*, *X-Ray Data Booklet* (Lawrence Berkeley National Laboratory, Berkeley, CA, 2009), 3rd ed.
[42] R. L. Cohen, G. K. Wertheim, A. Rosencwaig, and H. J. Guggenheim, Phys. Rev. B **5**, 1037 (1972).
[43] A. G. Kozorezov, C. J. Lambert, S. R. Bandler, M. A. Balvin, S. E. Busch, P. N. Nagler, J.-P. Porst, S. J. Smith, T. R. Stevenson, and J. E. Sadleir, Phys. Rev. B **87**, 104504 (2013).
[44] R. G. H. Robertson, Phys. Rev. C **91**, 035504 (2015).
[45] A. Faessler and F. Šimkovic, Phys. Rev. C **91**, 045505 (2015).
[46] A. Faessler, C. Enss, L. Gastaldo, and F. Šimkovic, Phys. Rev. C **91**, 064302 (2015).
[47] A. De Rújula and M. Lusignoli, J. High Energy Phys. 05 (2016) 015.